Int. J. Solids Structures, 1969, Vol. 5, pp. 573 to 586. Pergamon Press. Printed in Great Britain

STRESSES IN A PERFORATED RIBBED CYLINDRICAL SHELL SUBJECTED TO INTERNAL PRESSURE

A. J. DURELLI,* V. J. PARKS† and HAN-CHOW LEE‡

The Catholic University of America, Washington, D.C.

Abstract—This paper deals with an experimental determination of stresses in a perforated ribbed cylindrical shell subjected to internal pressure. Brittle coating, electrical strain gages, photoelasticity, and micrometers were used for the analysis. The results obtained were compared with a theoretical solution.

NOTATION

D	diameter of hole
E	modulus of elasticity
F_σ	model stress fringe value
L	half length of cylindrical shell
R	radius of cylindrical shell
c	spacing of ribs
n	fringe order
p	internal pressure
r	inner radius of ribs
t	thickness of cylindrical shell wall
t_0	thickness of ribs
ν	Poisson's ratio
$\sigma_{\theta\theta}$	hoop stress
σ_{zz}	longitudinal stress
$\varepsilon_{\theta\theta}$	hoop strain
ε_{zz}	longitudinal strain
r, θ, z	cylindrical coordinates

INTRODUCTION

THE problem of the stress distribution in a cylindrical shell stiffened by interior or exterior ribs subjected to various loadings has been studied theoretically and experimentally by several investigators [1–3]. In practical applications, particularly in the field of aircraft, ships and submarine structures, the shells are often perforated with a single hole or multiple holes. A survey of the papers on the use of various methods employed in studying stress concentrations near holes in shells may be found in a paper by Savin [4]. Recently Eringen and his associates [5] also made a theoretical analysis of a stiffened cylindrical shell with a circular hole under hydrostatic pressure.

The present work deals with the determination of stresses in a perforated ribbed cylindrical shell subjected to internal pressure. For the determination use is made of several experimental methods such as brittle coatings, strain gages and photoelasticity, which had already been employed in a previous study of a pressurized cylinder with a hole [6].

* Professor, Civil Engineering and Mechanics Department.
† Associate Professor, Civil Engineering and Mechanics Department.
‡ Post-Doctoral Fellow, Civil Engineering and Mechanics Department.

Both ends of the shell are capped and the internal pressure includes an axial component. Of primary interest in this investigation are the stresses around the hole, and the extent of the influence of the hole on the stresses in the shell. The results obtained are compared with a theoretical solution.

GEOMETRY AND LOADING

An epoxy cylindrical shell was machined from a 2 in. thick wall hollow cylinder cast using Hysol 4290. The geometry of the shell is indicated in Fig. 1. The plates at the end of the shell were made from an aluminum sheet.

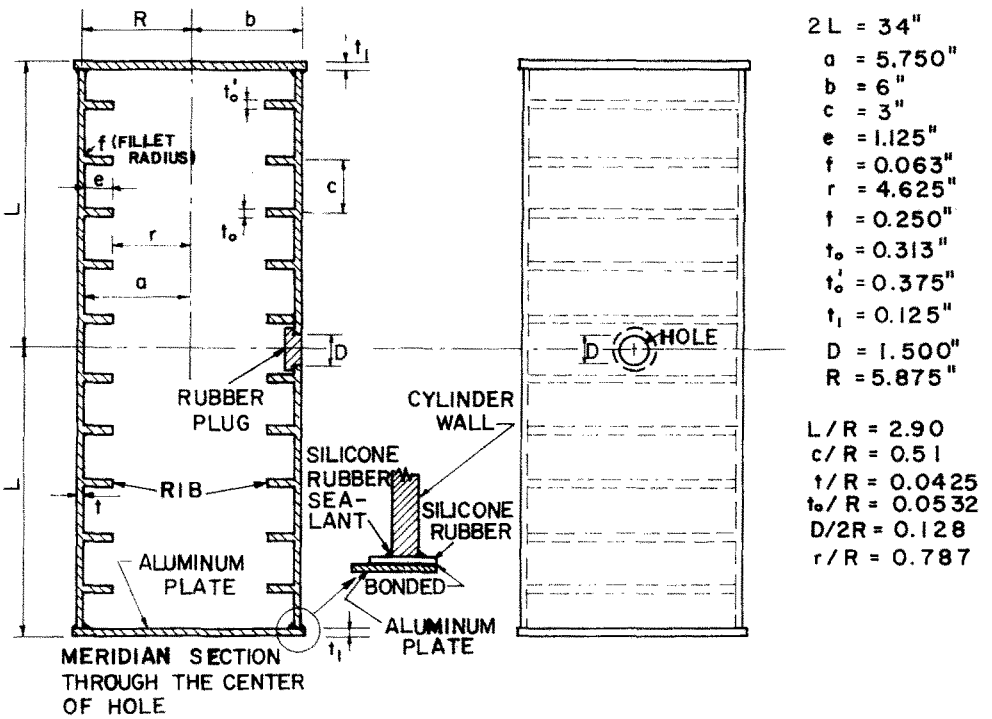

FIG. 1. Geometry of the epoxy perforated ribbed cylinder.

The dimensionless quantities defining the geometry are: $L/R = 2{\cdot}90$, $c/R = 0{\cdot}51$, $t/R = 0{\cdot}0425$, $t_0/R = 0{\cdot}0532$, $t_0'/R = 0{\cdot}0638$, $D/2R = 0{\cdot}128$, $r/R = 0{\cdot}787$ and $f/R = 0{\cdot}0106$, where R is the radius of the middle surface of the cylindrical shell, r is the inner radius of the ribs, $2L$ is the length of the cylindrical shell, c is the spacing between the ribs, t is the thickness of the cylindrical shell wall, t_0 is the thickness of all the ribs, except the two end ribs, t_0' is the thickness of the end ribs, D is the diameter of the hole, and f is the fillet radius between shell and rib.

The load applied to the ribbed cylindrical shell is uniform internal pressure. In order to contain the pressure a plug made of silicone rubber was attached as shown in Fig. 1.

The dimensions corresponding to the plug are shown in Fig. 2. It was kept in place by the pressure.

Two levels of internal pressure were used, 12 psi for the electrical strain gage test and 1·5 psi for the photoelasticity test.

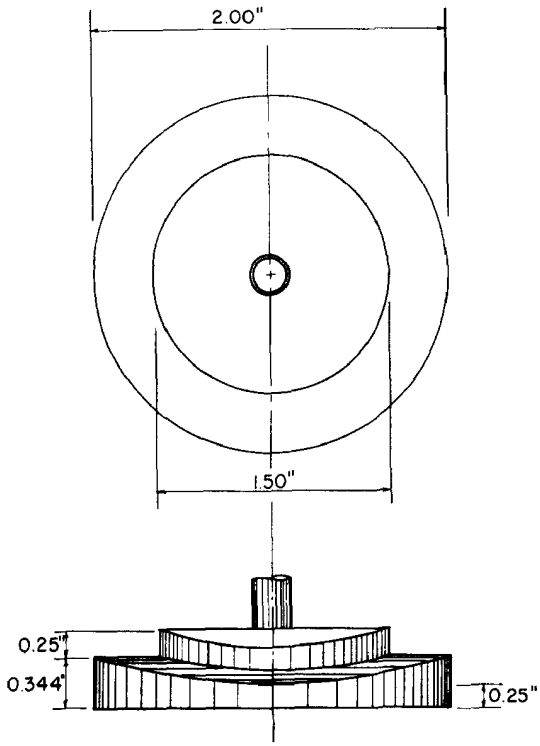

FIG. 2. Detail of the plug cast using silicone rubber.

NORMALIZATION OF DATA

In order to conveniently generalize the results it is customary to normalize the stresses by dividing them by some measure of the load which has the same units as the stresses. The simplest normalizing factor would be the pressure associated with the particular stress. However, in cases where a discontinuity such as the hole is introduced in an otherwise uniform field (the plain cylinder) it is customary to normalize stresses in terms of one of the stresses present in the uniform portion of the shell. This gives an indication of the factor by which the hole increases the stress.

In the geometry analyzed here there is no "uniform" stress region in the shell because of the presence of the ribs. However, the stresses throughout the shell are still highly dependent on the same geometric values (shell radius and shell wall thickness) that would determine the stress if there were no hole and no ribs. The average longitudinal stress between the ribs and away from the hole must still satisfy equilibrium and is $\sigma_{zz})_{av} = pR/2t$. Except for the restraint of the ribs, the average hoop stress away from the hole would be

$\sigma_{\theta\theta})_{av} = pR/t$. It was decided to normalize all the results on the factor pR/t to emphasize the effect of ribs and hole, and to be compatible with the previous work [6] in which the stresses were normalized with respect to $\sigma_{\theta\theta}$ in a uniform section.

EXPERIMENTAL WORK AND ANALYSIS

Brittle coating

The brittle coating method uses a thin layer of a brittle varnish-like material sprayed on a specimen where surface stresses are to be determined. The strains occurring on the surface of the specimen, due to loading, are transmitted to the coating. When these strains produce stresses in the coating larger than its ultimate strength, the coating fails by cracking. The cracks are perpendicular to the tensile stress producing failure, therefore they coincide with the isostatics or principal stress trajectories and give the direction of the principal stresses directly. To determine the value of stresses the cracking failure of the coating is associated with the strain sensitivity of the coating obtained by calibration following a procedure developed elsewhere [7] and described below.

The coating was sprayed on the surface of the shell in a number of passes, with several minutes between each pass. Stresscoat coating No. ST-1207 was used. The shell was prepared for pressurizing immediately after spraying and the coating cured in place. The test was conducted about 20 hours after spraying.

The brittle coating under load relaxes its stress making it necessary to apply the load to the specimen sufficiently fast in order to crack the coating. It is also necessary to remove the load after a short time to prevent "relaxation" cracking and to wait several minutes between loadings to allow the coating to return to the no-load state.

Loads were applied to the shell with a column of mercury (similar to that shown in Fig. 4), in from 60 to 90 sec, held for 15 sec, and reduced to zero in approximately the same time it took to apply the load. After each load application, the entire coating surface was carefully examined for cracks (isostatics). The load level was increased by steps until the first cracks appeared in the coating. The cracks were encircled by a line made with a soft marking pencil and the line assigned a code number corresponding to the value of load at which the cracks appeared. With each subsequent load, the growth of the isostatic pattern was again bounded and numbered, so that a series of contour lines resulted. The contour lines are known as isoentatics. An isoentatic (locus of the crack ends) represents a line of constant "apparent" stress. The stress is called "apparent" in that it neglects the influence of the secondary stresses, gradient of stress, etc. on the failure of the coating. As a first approximation, this "apparent" stress can be taken as the maximum stress at the point.

Upon completion of the test, the isoentatics and code numbers were marked over with a fine steel scribe. The coating was then treated with red dye etchant which colors the isostatics and isoentatics and contrasts them with the yellow coating. Photographs of the pattern were taken to establish permanent records of the tests. The photograph shown in Fig. 3 was obtained by attaching a large sheet of negative film to the outer surface of the shell, in the neighborhood of the hole, with the sensitive side in contact with the brittle coating. A white-light source was put on the opposite side of the shell with respect to the hole. The shell itself acted as a diffuser.

In Fig. 3 the location of the isotropic points for the outer surface of the shell are shown (points at which equal tensile stresses are present in all directions on the surface). The crack

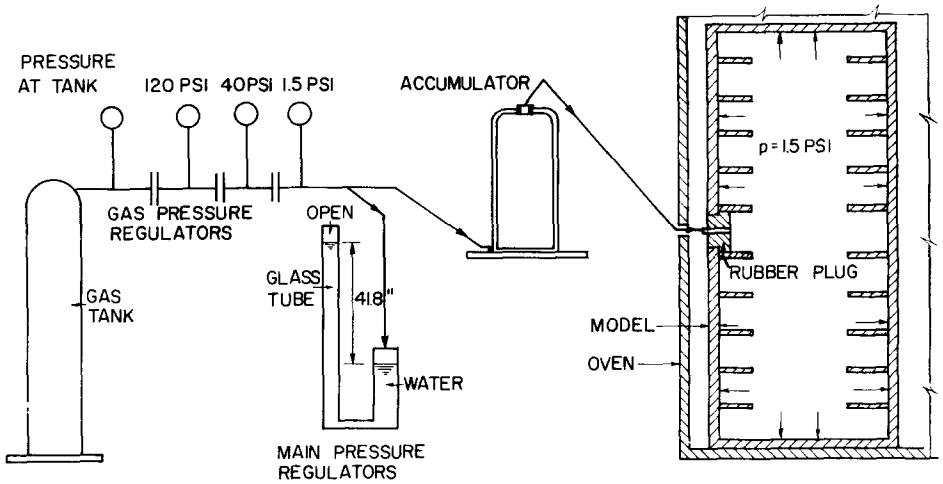

FIG. 4. Method of applying internal pressure to perforated ribbed cylinder.

pattern as shown in Fig. 3 was extended beyond the last isoentatics (No. 7) by using the refrigeration technique as explained elsewhere [7] to obtain isostatics over the whole surface. A fairly regular pattern has been obtained in the region away from the discontinuity except for the presence of some irregular cracks, which were produced by local lack of uniformity of temperature when the coating was refrigerated.

The normalized apparent stresses are obtained from

$$\left.\frac{\sigma}{pR/t}\right|_i = \frac{E\varepsilon}{p_i}\left(\frac{t}{R}\right), \tag{1}$$

where σ is the apparent stress at isoentatic i when a p_i pressure is applied to the shell, which produced failure (cracking) of the coating up to isoentatic i, ε is the strain sensitivity of the coating obtained from the calibration strips and E is Young's modulus of the shell material.

If the coating failed at a specific tensile stress and if the Poisson's ratio of coating and shell were the same then this relation would give the maximum principal stress σ_1 in the shell regardless of the biaxial conditions of the specimen. It is known that the coating does fail at a somewhat lower load if the specimen is in a state of biaxial tension. The coating failure is also influenced to some degree by the stress gradient in the shell and to a lesser degree by change in coating thickness. Because of these influences the value obtained for stress is specified as "apparent" and is estimated to vary some ± 15 per cent from the true stress.

Electrical strain gages

At two points away from the hole, midway between two ribs, sets of four electrical strain gages (Metafilm Strain Gages C6-111 and C6-121) were mounted (two on the inner surface and two on the outer surface in the principal directions). A set of two gages were also mounted on the outer surface directly over a rib and one gage was mounted circumferentially on the inner radius of the rib. A pressure of 12 psi was applied. The

electrical strain gages were used mainly to obtain precise strain readings in the regions of low strain and to check data given by the other procedures.

The directions of all seven gages coincided with the lines of symmetry of the cylinder. The stresses were computed from these strain measurements using Hooke's law:

$$\sigma_{zz} = \frac{E}{1-\nu^2}(\varepsilon_{zz} + \nu\varepsilon_{\theta\theta}), \tag{2}$$

$$\sigma_{\theta\theta} = \frac{E}{1-\nu^2}(\varepsilon_{\theta\theta} + \nu\varepsilon_{zz}), \tag{3}$$

where σ_{zz} is the longitudinal stress on the surface, $\sigma_{\theta\theta}$ is the hoop stress on the surface, ε_{zz} is the longitudinal strain on the surface, $\varepsilon_{\theta\theta}$ is the hoop strain on the surface, and ν is Poisson's ratio (a value of 0·36 was used in this strain gage evaluation).

In the case of the single gage on the inner radius of the rib, the relation reduces to $\sigma_{\theta\theta} = E\varepsilon_{\theta\theta}$. Stress values obtained were again normalized with pR/t.

Photoelasticity

The "freezing" method was used. The shell was put inside an oven and the temperature was raised up to 270°F at a rate of 1°F/hr. The temperature was kept constant at 270°F for about 8 hr. One hour after reaching this state a pressure of 1·0 psi was applied, and 3 hr later the pressure was increased to 1·5 psi. (The device used to apply the load and to measure and maintain it is shown in Fig. 4.) The temperature was brought down to 200°F at a rate of 1°F/hr. The rate was increased to 1·5°F/hr until reaching room temperature. The shell was unloaded and a total of 25 slices and sub-slices were removed. The thickness of the slices and their location are indicated in Fig. 5. Isochromatic patterns are shown in Figs. 6 and 7.

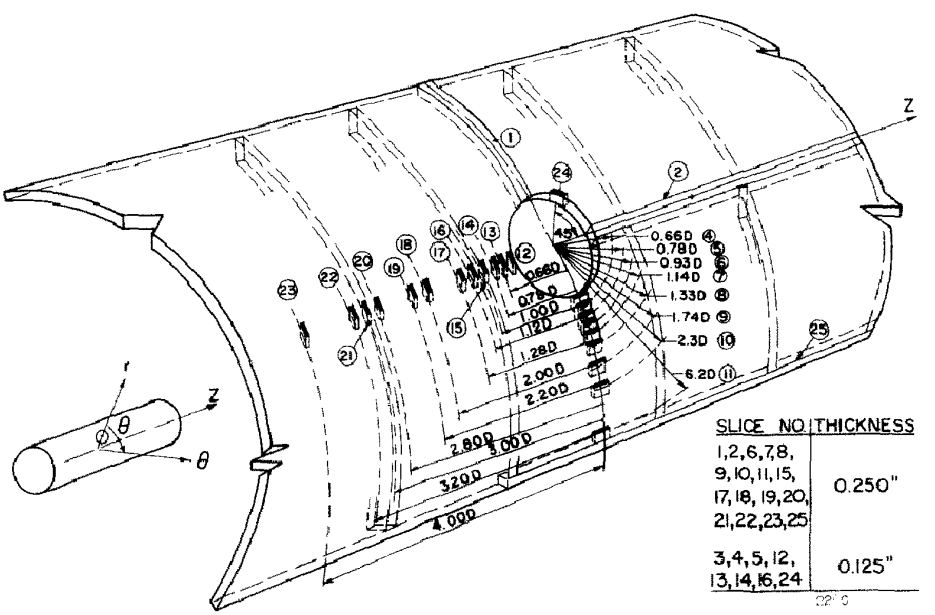

FIG. 5. Plan of the slices and sub-slices removed from the frozen epoxy perforated ribbed cylinder subjected to internal pressure.

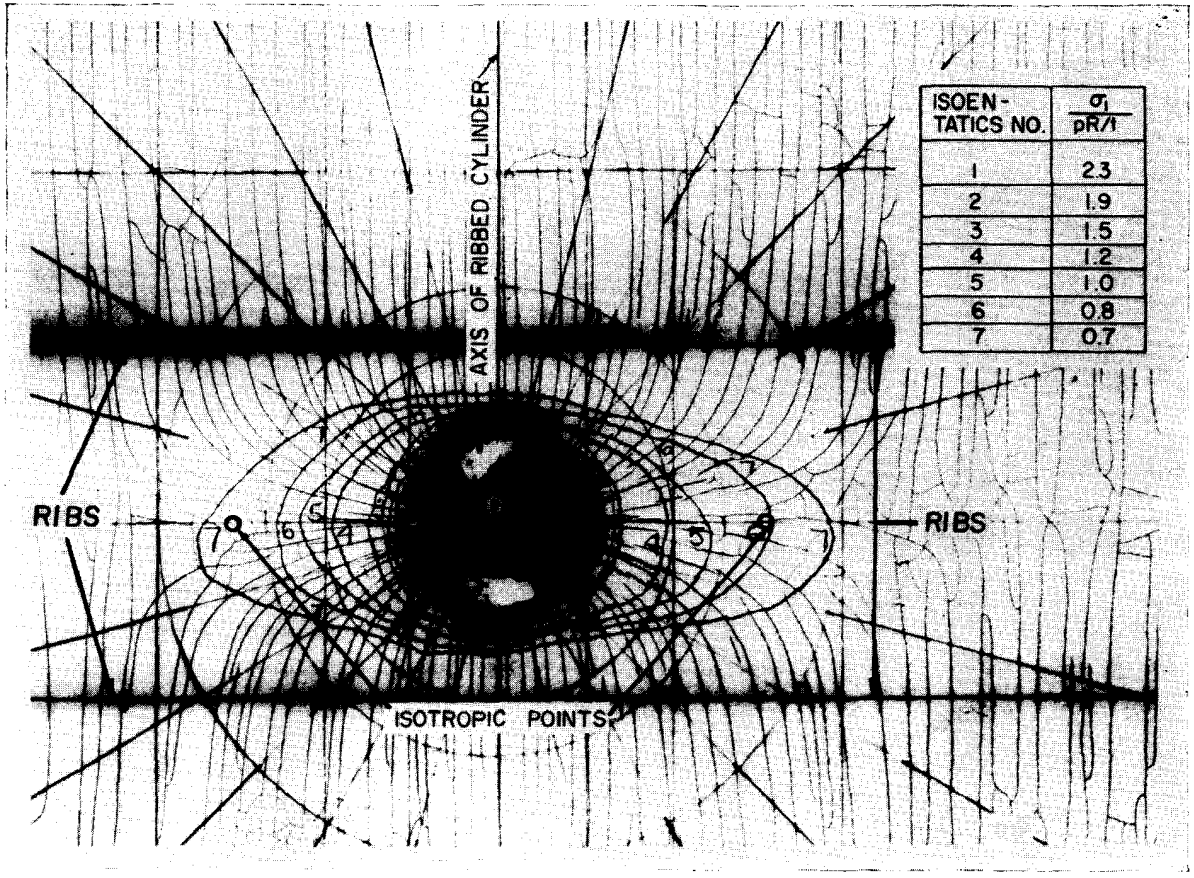

FIG. 3. Isostatics on the outer surface of the perforated ribbed cylinder subjected to internal pressure, in the neighborhood of the hole, obtained by means of a brittle coating.

[facing p. 578

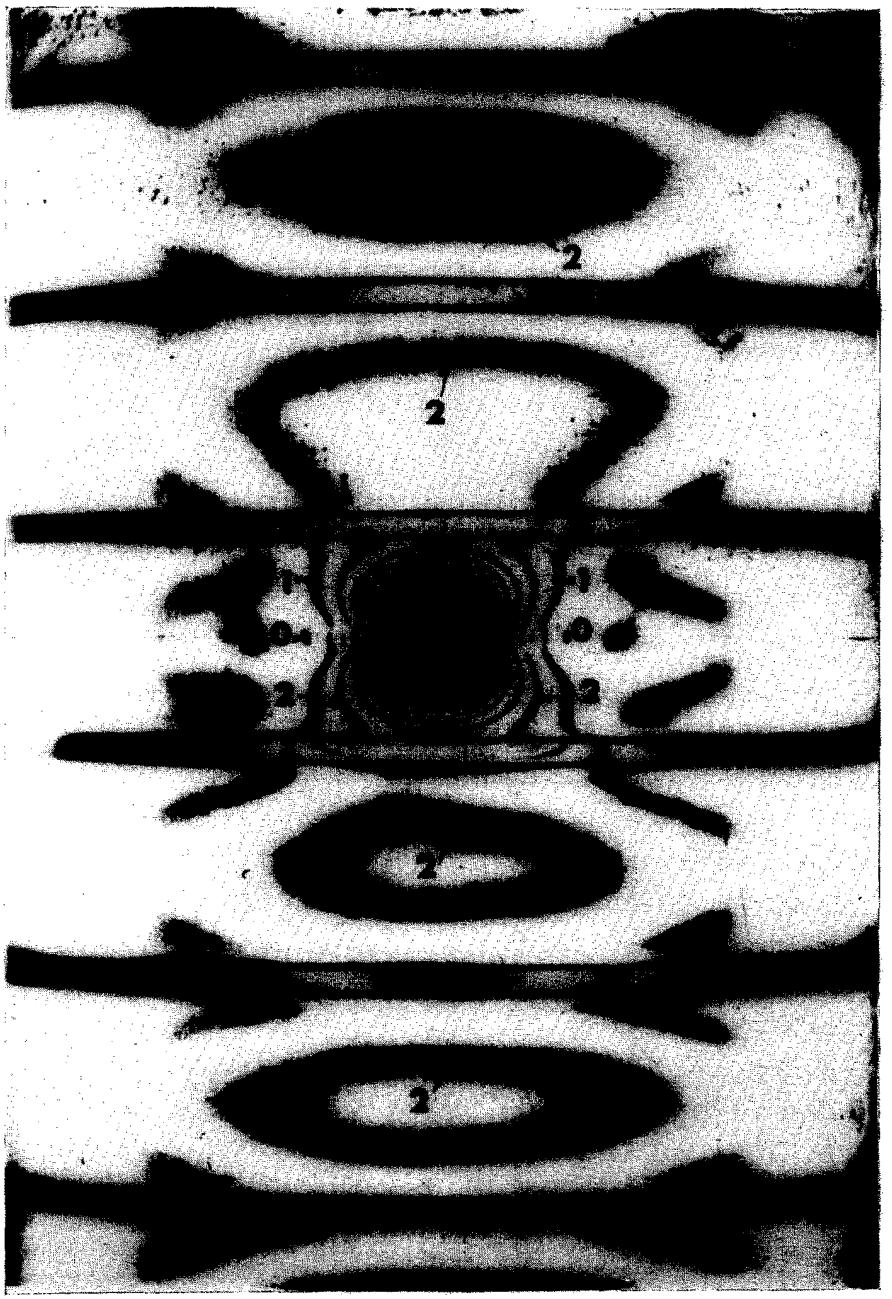

FIG. 6. Isochromatic pattern for a perforated ribbed cylinder subjected to internal pressure.

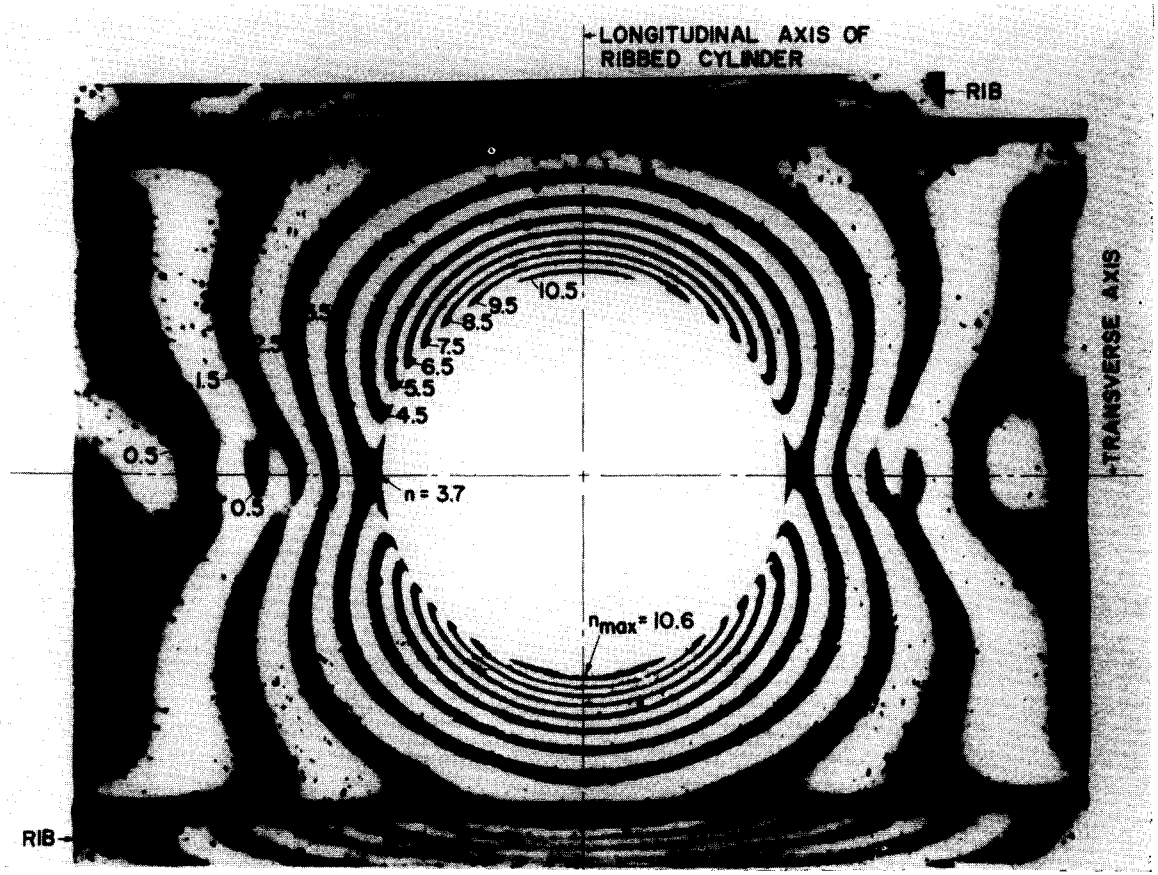

FIG. 7. Isochromatics around the hole in a ribbed cylinder subjected to internal pressure (t = 0·250 in.).

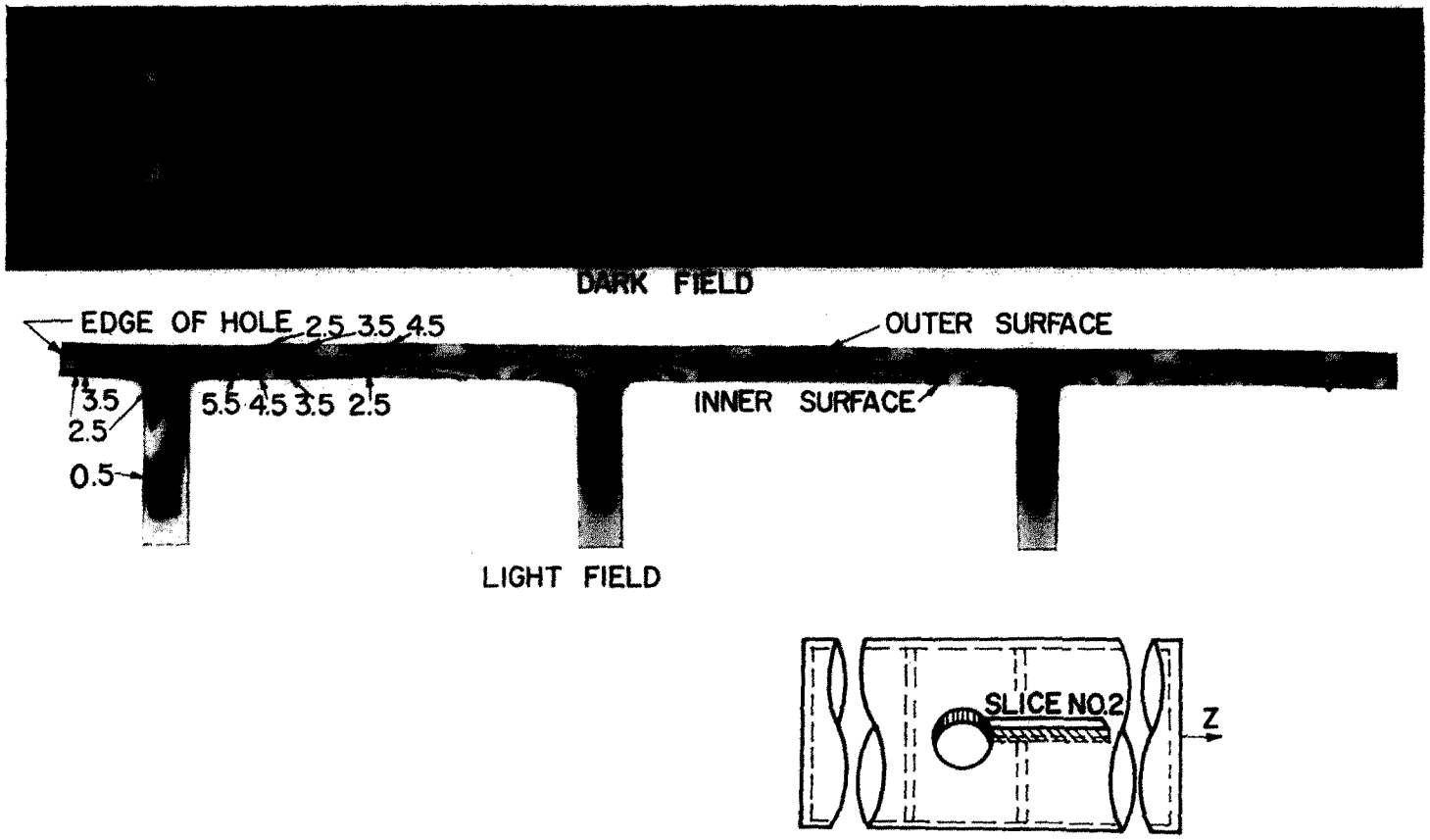

FIG. 8. Isochromatics in slice No. 2 ($t = 0{\cdot}250$ in.).

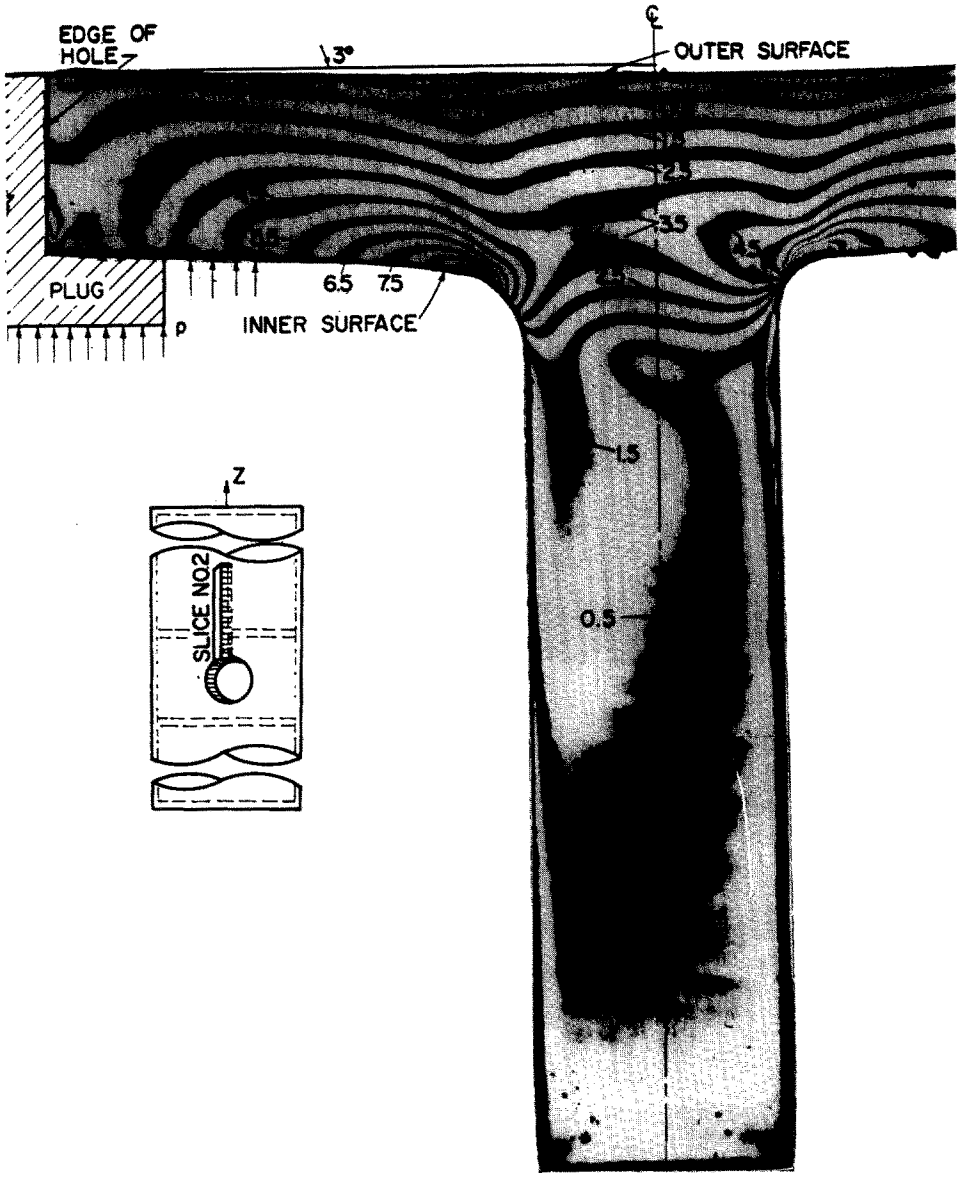

FIG. 9. Enlargement of isochromatics in the neighborhood of the hole in slice No. 2 ($t = 0{\cdot}250$ in.).

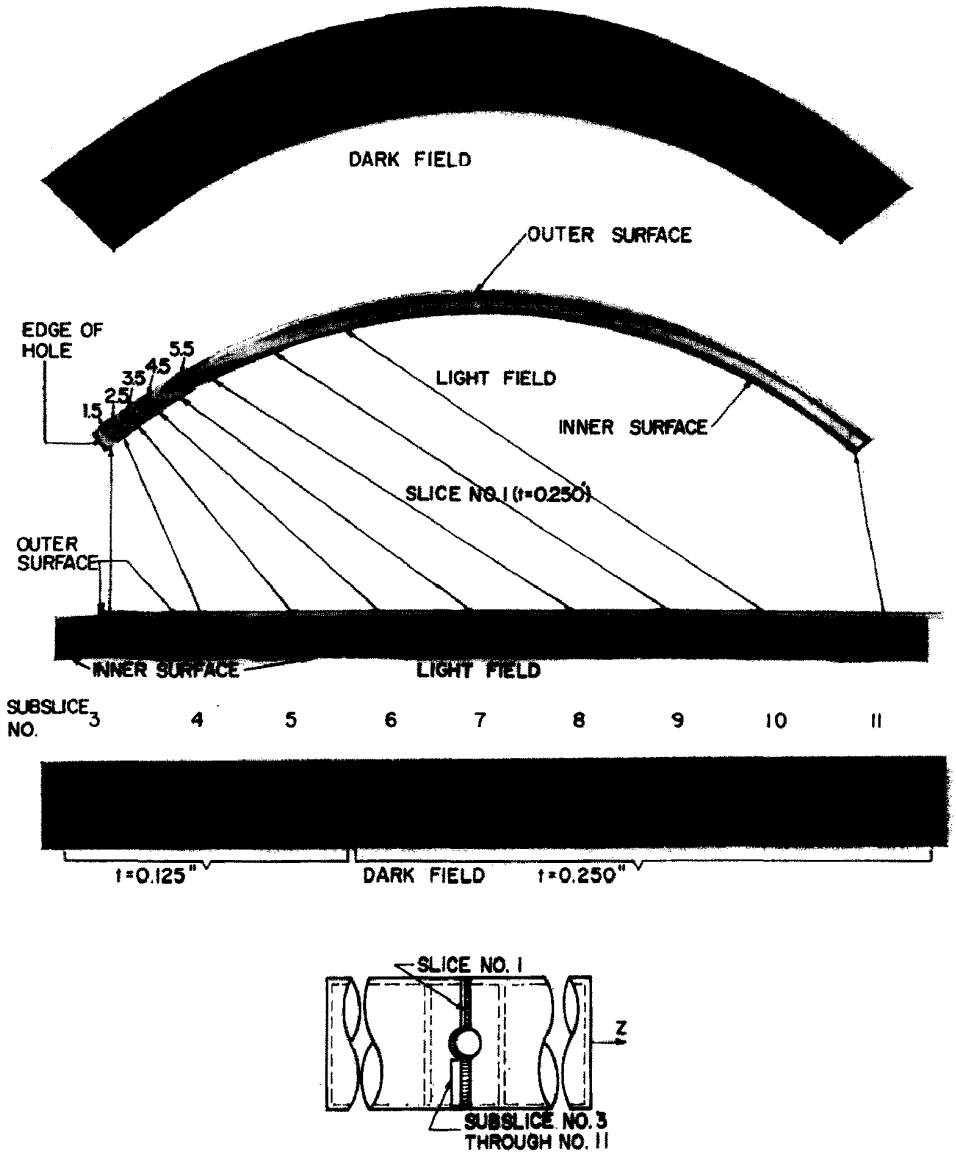

FIG. 10. Isochromatics in slice No. 1 and sub-slice No. 3 through No. 11.

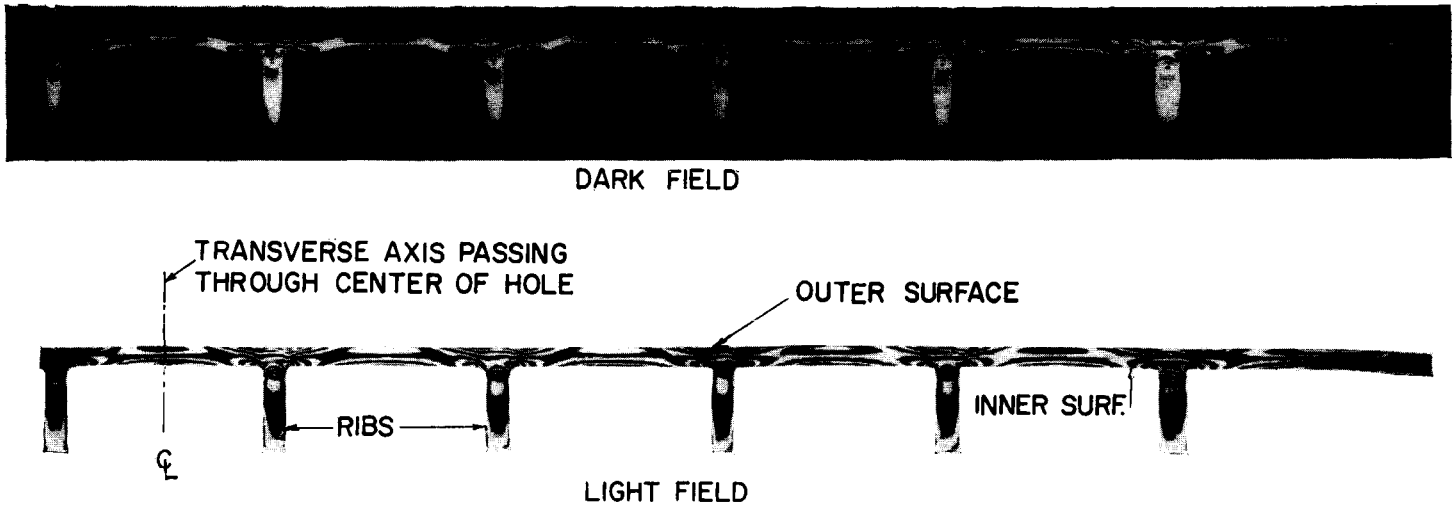

FIG. 11. Isochromatics in slice No. 25 ($t = 0{\cdot}250$ in.).

The over-all isochromatic pattern seen through the shell is shown in Fig. 6 (dark field). This pattern although indicating the general response is difficult to analyze in a quantitative manner, a light-field detail of the same pattern is shown in Fig. 7. Typical isochromatics of the slices used for analysis are shown in Figs. 8, 9 and 10. Most of the photoelastic analysis was done by photographing the slices in the polariscope and compensating to obtain fractional fringe orders using Tardy's method. Figure 11 is an isochromatic pattern, away from the hole, shown to indicate the regularity of the distribution from bay to bay.

Slices and sub-slices removed from the shell along two axes of symmetry near the hole were analyzed to obtain two principal stress components, namely, the hoop-stress and the longitudinal stress. These axes are: one parallel to the axis of the cylindrical shell (axis of slice No. 1), and the other perpendicular to it through the center of the hole (axis of slice No. 2). The tangential stresses along the boundary of the hole was also analyzed. The photoelastic analysis gives for points on the outer surface of slices or sub-slices:

$$\sigma_{\theta\theta} = 2nF_{\sigma}, \tag{4}$$

$$\sigma_{zz} = 2nF_{\sigma}, \tag{5}$$

and for points on the inner surface of slices or sub-slices:

$$\sigma_{\theta\theta} = 2nF_{\sigma} - p, \tag{6}$$

$$\sigma_{zz} = 2nF_{\sigma} - p, \tag{7}$$

where n is the observed fringe order at points corresponding to evaluated stress components on the surface of slices, for $t = \frac{1}{4}$ in. (thickness of slice), F_{σ} is the material fringe value corresponding to a thickness $t = \frac{1}{4}$ in. (A value of 2·65 psi per fringe was obtained from a calibration disk), and p is the applied internal pressure.

The normalized stresses are obtained by dividing equations (4) through (7) by the factor pR/t

$$\frac{\sigma_{\theta\theta}}{pR/t} = \frac{n}{6{\cdot}8}, \tag{8}$$

$$\frac{\sigma_{zz}}{pR/t} = \frac{n}{6{\cdot}8}, \tag{9}$$

for the outer surface, and

$$\frac{\sigma_{\theta\theta}}{pR/t} = \frac{n}{6{\cdot}8} - 0{\cdot}04, \tag{10}$$

$$\frac{\sigma_{zz}}{pR/t} = \frac{n}{6{\cdot}8} - 0{\cdot}04, \tag{11}$$

for the inner surface.

For points along the edge of the hole a similar photoelastic analysis gives

$$\sigma_{\tan} = 2nF_{\sigma}, \tag{12}$$

for the outer boundary, and

$$\sigma_{\tan} = 2nF_{\sigma} - p, \tag{13}$$

for the inner boundary, where σ_{tan} is the tangential stress along the edge of the hole. Stress values obtained here were again normalized dividing by pR/t.

Telescoping gage and micrometer

The change in diameter of the middle surface of the boundary of the hole was obtained by a series of readings made with a telescoping gage and micrometer. The change in diameter of the shell in uniform regions midway between the ribs and over the ribs was also measured with a large micrometer. All these readings were obtained to within 0·001 in. before and after loading the shell in the oven.

The change in diameter of the outer surface $\Delta D/D$ was 0·00602 on the rib and 0·00811 on the center between the ribs.

RESULTS

An approximate field of σ_1, on the outer surface around the hole is given directly by the brittle coating shown in Fig. 3. Normalized stresses for points on the outer and inner surfaces of the shell, along the two lines of symmetry (obtained using brittle coating, strain gages and photoelasticity) are given in Figs. 12 to 15. The distribution of the membrane stresses at the boundary of the hole (from the photoelasticity pattern in Fig. 7) is shown in Fig. 16. The projection of the middle surface of the boundary of the hole, before and after deformation, on a plane perpendicular to a radial line through the center of the hole (obtained from the telescope gage and micrometer) is also given in Fig. 16. The distribution

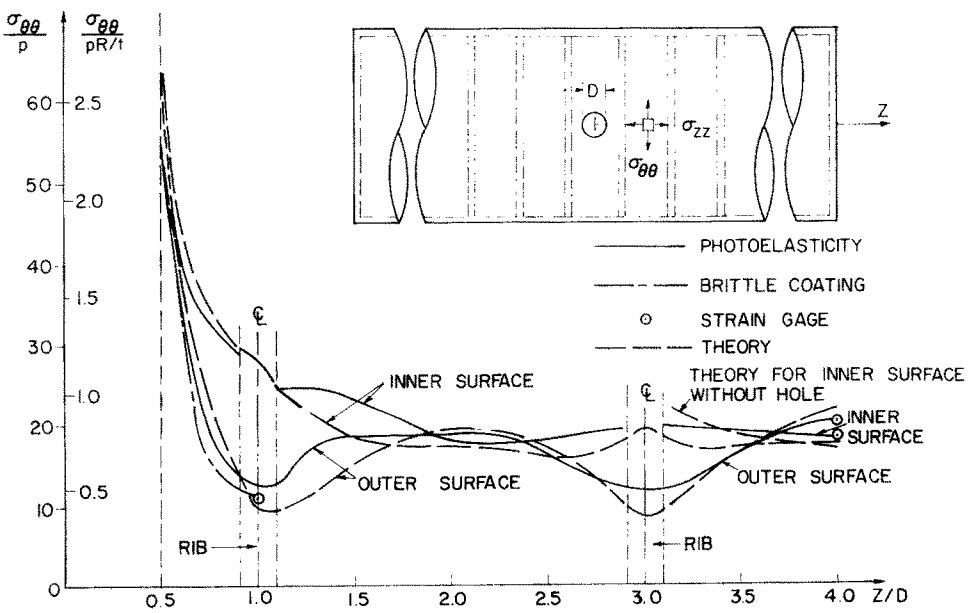

FIG. 12. Hoop stresses along the longitudinal axis of the perforated ribbed cylinder subjected to internal pressure.

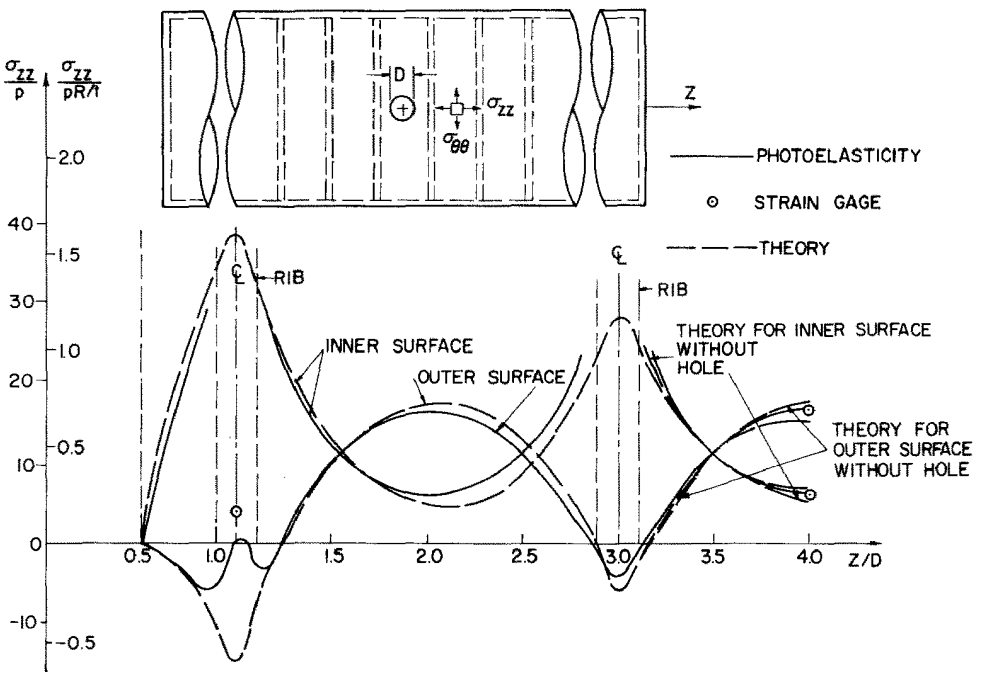

FIG. 13. Longitudinal stresses along the longitudinal axis of the perforated ribbed cylinder subjected to internal pressure.

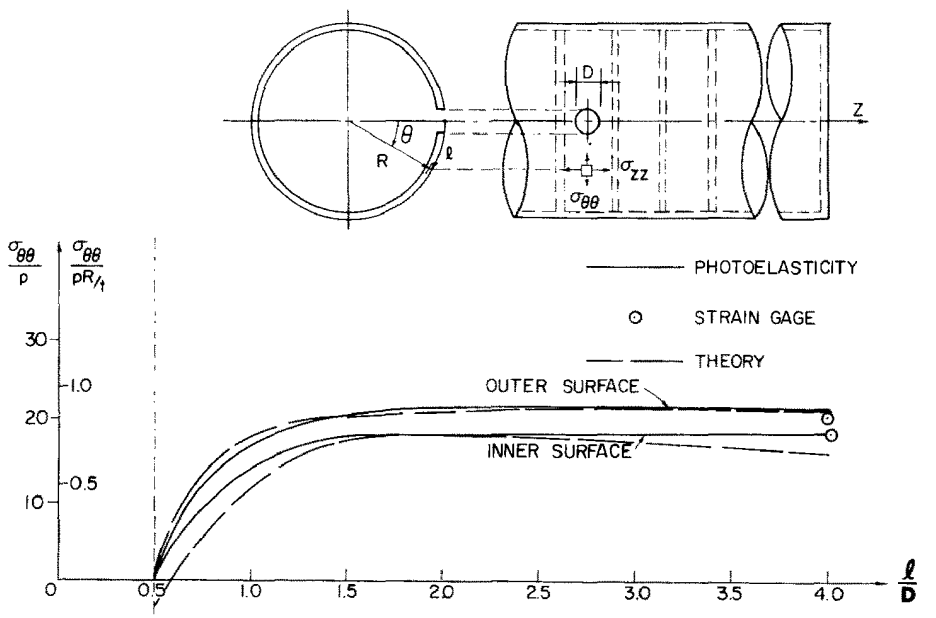

FIG. 14. Hoop stresses along the transverse axis of the perforated ribbed cylinder subjected to internal pressure.

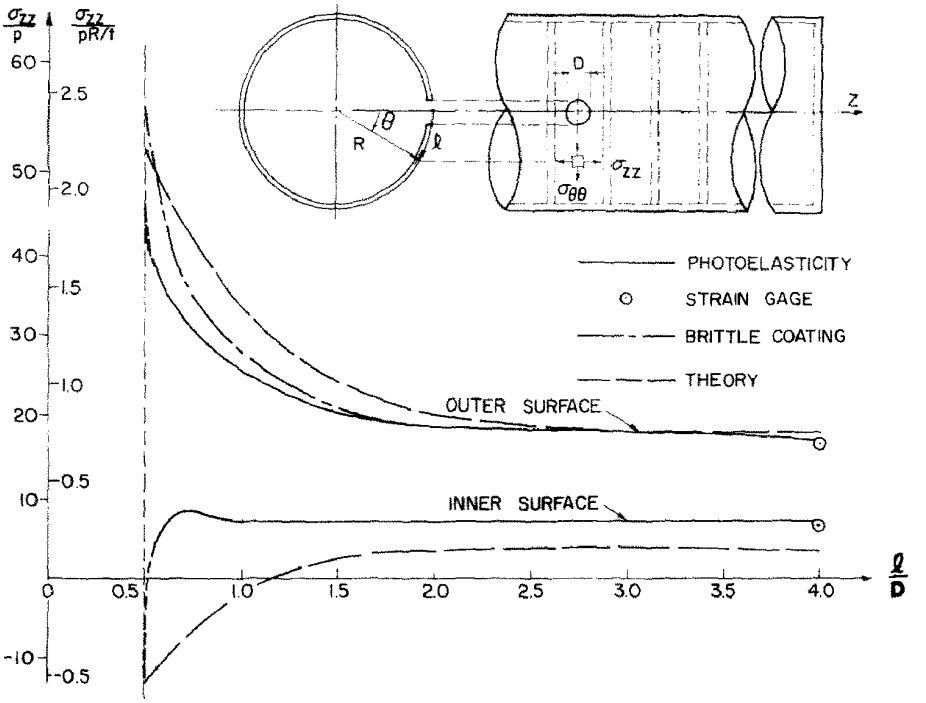

FIG. 15. Longitudinal stresses along the transverse axis of the perforated cylinder subjected to internal pressure.

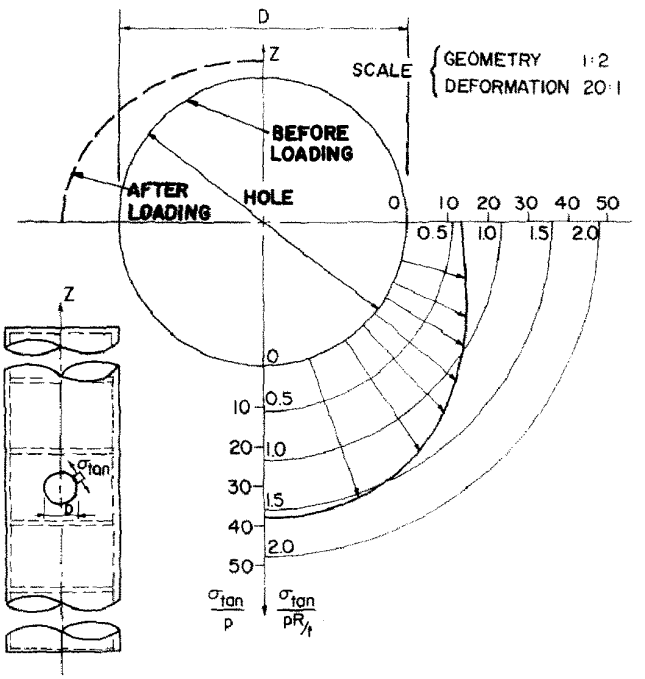

FIG. 16. Normalized membrane stresses and deformation at the edge of the hole in the ribbed cylinder subjected to internal pressure.

of the stresses at the inner and outer surfaces along the boundary of the hole (from photoelasticity and brittle coating) are shown in Fig. 17. The distribution of the tangential stresses at the corner between cylinder wall and rib and the hoop stress along the rib (from photoelasticity) are plotted in Fig. 18.

The distribution of stresses in a ribbed cylindrical shell without any perforations subjected to internal pressure may also be of interest. Both the hoop stresses and the longitudinal stresses at points away from the hole along the longitudinal axis obtained in the analysis give the solution to this problem. These stress distributions can be found in Figs. 12 and 13 beyond the second rib away from the center of the hole (i.e. $3{\cdot}0 \leq z/D \leq 4{\cdot}0$). The influence of the hole in this region is negligible. The stresses are symmetrical with respect to the center line between two adjacent ribs.

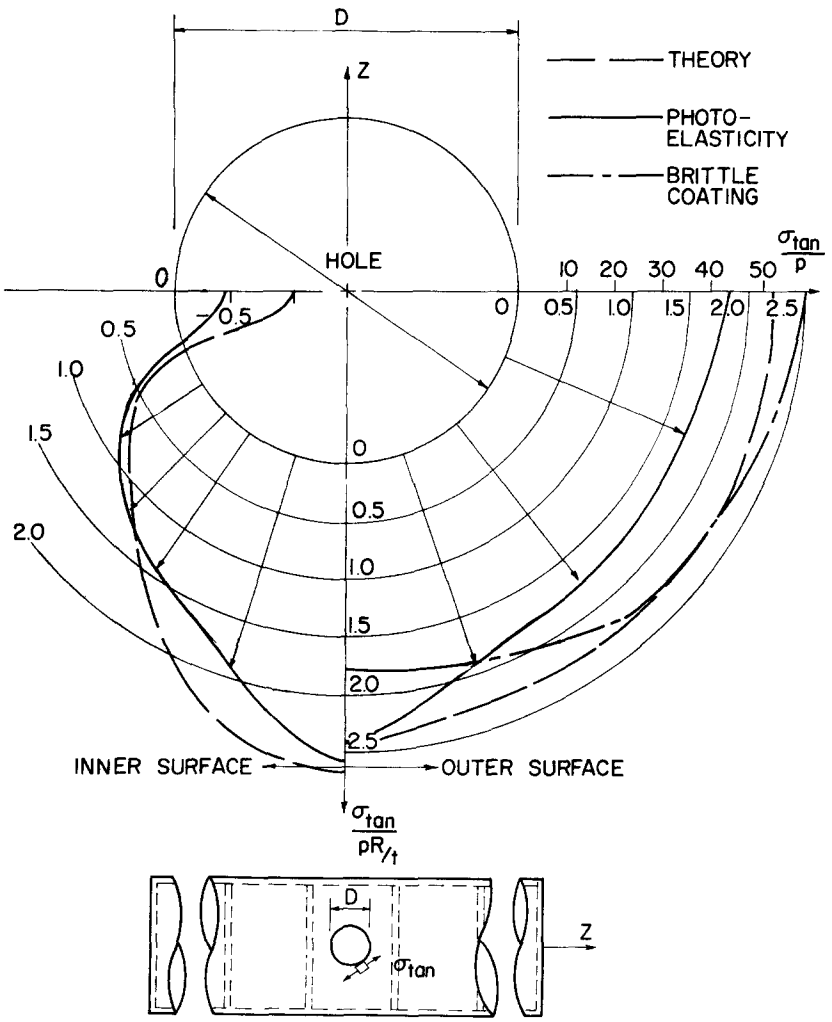

FIG. 17. Normalized stresses (bending + membrane) at the outer and inner surfaces at the boundary of the hole in the ribbed cylinder subjected to internal pressure.

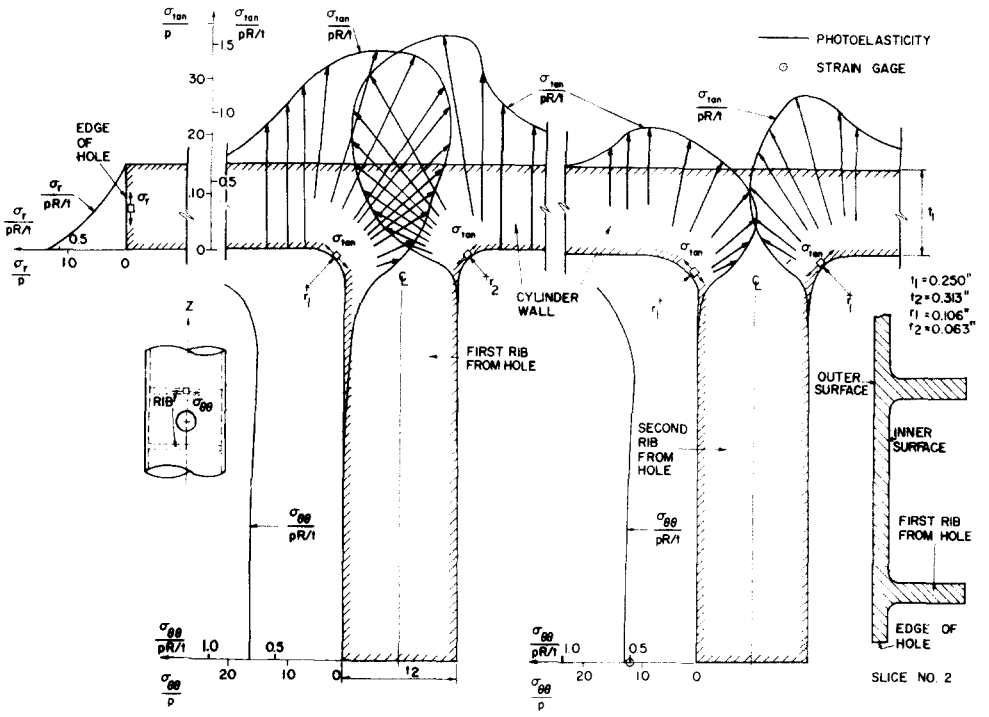

FIG. 18. Normalized tangential stresses at the corner between cylinder wall and rib, and hoop stresses along the rib in the perforated ribbed cylinder subjected to internal pressure.

The stress distributions obtained in this analysis may be compared with a theoretical solution given by A. C. Eringen [5] for the case of a cylindrical shell stiffened with two ribs on each side of the hole.* Curves obtained using this theoretical solution are shown in Figs. 12 to 15 and 17. General agreement was obtained except in the neighborhood of the ribs, and at the edge of the hole where the deviation between the results obtained by the experiment and the theoretical solution was found to be appreciable. It should be noted that the case analyzed experimentally is not identical to the case considered in the theory. In the theoretical solution, the boundary of the hole is subjected to shear load, while in the experiment there are normal forces applied along the contour of the hole at the inner surface of the shell. In the theoretical solution, the shell is stiffened with two ribs only, while in the experiment the shell is stiffened with five ribs on each side of the hole. The discrepancies between the experimental result and the theoretical solution seem to be more likely due to the difference in the boundary conditions of the hole rather than in the number of ribs.

For the region $3{\cdot}0 \leq z/D \leq 4{\cdot}0$ as mentioned above the influence of the hole is negligible, therefore, the results obtained here may be compared with another theoretical solution [8] for the case of a ribbed cylindrical shell with no hole, as also shown in Figs. 12 and 13. The comparison with the experimental results is satisfactory.

The results obtained from brittle coating and photoelasticity show that there are some discrepancies between the two methods in particular along the boundary of the hole (Fig. 17).

* This solution was evaluated for the particular parameters of this investigation by Oles Lomacky of the Naval Ship Research and Development Center using a computer.

The ratio of moduli of elasticity of epoxy and plug varies greatly between room temperature ($E_e/E_r = 500$) and "freezing" temperature ($E_e/E_r = 2$). This may influence the distribution of load between the plug and the model and so account for the discrepancies that were noted.

The photoelastic results at the point midway between two ribs in the second bay from the hole along the longitudinal axis and at the point at 90° circumferentially from the hole along the transverse axis checked with those obtained from strain gage measurements. Another check in the photoelastic analysis can be also obtained by comparing the difference of average principal stresses obtained directly from the over-all isochromatics before slicing (Fig. 6) and the difference of the same stress from the axial slice and transverse sub-slices. Both checks have been applied to the same points. Good agreement has been obtained.

The accuracy of the photoelastic determinations was evaluated from several points of view. Besides the slices mentioned above, other longitudinal slices were removed from the shell and the results obtained from spans located in similar positions with respect to the end and the hole, were compared. The results obtained from points which ideally should have the same value of stress show no more than 4 per cent discrepancy from their average. Other sources of error like the ones associated with the machining of the specimen have also been considered, hence the parasitic edge effects. Using previous experience with these experimental observations it is believed that the true values will fall within a range determined by the given values ± 6 per cent.

DISCUSSION

The most striking feature of the analysis seems to be the localized influence of the hole. This influence is confined almost completely to the bay in which the hole is located. Both the brittle coating results (Fig. 3) and the photoelastic results (Fig. 6) show clearly this localization which has been also found theoretically [5]. The quantitative analysis confirms that the influence of the hole on the stresses in the adjacent two bays is small. The influence of the hole on the stresses along the circumferential direction of the shell is about the same as that found in the shell with no ribs [6].

Acknowledgments—The authors would like to express their appreciation to the Naval Ship Research and Development Center for the opportunity of contributing to the solution of an important problem. In particular, they would like to acknowledge the cooperation and understanding of Dr. Oles Lomacky in the development of the research program.

Mr. H. E. Miller machined the model and cut out the slices. Mr. J. F. McDonough made the drawings and Mrs. G. M. Howser was in charge of the typing. The authors would like to acknowledge these contributions.

REFERENCES

[1] K. G. MANTLE, N. MARSHALL, P. J. PALMER. Experimental investigation into the stress distribution in a band-reinforced pressure-vessel. *Proc. Inst. mech. Engrs* **173**, 123 (1959).

[2] D. S. HOUGHTON, Optimum design of a band reinforced pressurized cylinder. *The College of Aeronautics, Cranfield, England, Note No.* 116 (April 1961).

[3] P. A. ZHILIN, Axisymmetric strain of a rib-reinforced cylindrical shell. *Mekh. Tverdogo. Tel. No.* 5, 139–142 (1966).

[4] G. N. SAVIN, *Trudy* II *Vsesoyuznoy Konferentsii po teorii obolochek i plastin. (Proc. 2nd All-union Conf. Shell Plate Theory)*. Kiev, Izdatel'stvo Akademii Nauk USSR (1962).

[5] M. M. STANISIC, J. A. EULER, E. H. DOWELL, and A. C. ERINGEN, Stress distribution in a stiffened circular cylindrical shell with a circular cutout under hydrostatic pressure. *Tech. Report No.* 7–1, *General Technology Corp.* (August 1967).
[6] A. J. DURELLI, C. J. DEL RIO, V. J. PARKS, and H. FENG, Stresses in a pressurized cylinder with a hole. *J. Struct. Div. Am. Soc. civ. Engrs* **93**, No. ST-5, 383–399 (October 1967).
[7] A. J. DURELLI, E. A. PHILLIPS, and C. H. TSAO, *Introduction to the Theoretical and Experimental Analysis of Stress and Strain* McGraw-Hill (1958).
[8] V. L. SALERNO and J. G. PULOS, Stress distribution in a circular cylindrical shell under hydrostatic pressure supported by equally spaced circular ring frames. *Polytechnic Institute of Brooklyn, Aeronautical Laboratory, Report No.* 171-*A* (June 1951).

(*Received* 2 *August* 1968; *revised* 23 *October* 1968)

Абстракт—Работа занимается экспериментальным определением напряжений в перфорированной ребристой цилиндрической оболочке, подверженной внутреннему давлению. Для анализа оболочки используются хрупкое покрытие, электрические датчики деформаций, фотоупругость и микрометры. Полученные результаты сравниваются с теоретическим решением.